

# Robust data processing of noisy marine controlled-source electromagnetic data using independent component analysis

Naoto Imamura<sup>1,5</sup> Tada-nori Goto<sup>2,4</sup> Takafumi Kasaya<sup>3</sup> Hideaki Machiyama<sup>4</sup>

<sup>1</sup>College of Earth, Ocean, and Atmospheric Sciences, Oregon State University, 104 CEOAS Administration Building, Corvallis, OR 97331-5503, USA.

<sup>2</sup>Graduate School of Engineering, Kyoto University, C1-2-216, Kyotodaigaku Katsura, Nishikyo-ku, Kyoto-shi 615-8540, Japan.

<sup>3</sup>Research and Development Center for Earthquake and Tsunami, Japan Agency for Marine-Earth Science and Technology (JAMSTEC), 2-15 Natsushima, Yokosuka, Kanagawa 237-0061, Japan.

<sup>4</sup>Research and Development Center for Submarine Resources, JAMSTEC, 2-15 Natsushima, Yokosuka, Kanagawa 237-0061, Japan.

<sup>5</sup>Corresponding author. Email: [nimamura@ceoas.oregonstate.edu](mailto:nimamura@ceoas.oregonstate.edu)

**Abstract.** Data processing techniques are often used to estimate the noise-free response of marine controlled-source electromagnetic (CSEM) data and magnetotelluric transfer functions. We have implemented a new CSEM data processing scheme that uses a robust method based on independent component analysis (ICA) to extract interpretable datasets from noisy marine CSEM data. We applied the data processing scheme to signals from a new CSEM observation system comprising a remotely operated vehicle (ROV) and an ocean bottom electromagnetometer (OBEM). These datasets were obtained around the Iheya North hydrothermal field, Okinawa Trough, Japan. The observation system allows a small-scale CSEM survey to be conducted in areas of steep topography, such as hydrothermal fields, because the ROV can deploy the OBEM at the exact observation site. The results show that the coherent and environment noise that exists in the raw time series is reduced sufficiently by ICA processing. It makes interpretation of the resulting electric field data possible. The results also show that the processed data has a higher signal-to-noise ratio in the middle-to-high-frequency band than the data without ICA. The normalised spectrum, obtained by normalising the observed data from the hydrothermal area, indicates that a conductive anomaly exists in the near-offset area around the OBEM. We apply 2D inversion to the electric field data and find that a low resistivity body exists beneath the OBEM and 50 m offset from the OBEM. This resistivity structure is consistent with images taken by the ROV that show characteristic organisms in hydrothermal seepage around the OBEM site.

**Key words:** controlled-source electromagnetic method, hydrothermal vent, independent component analysis, Okinawa Trough, robust data processing.

Received 23 October 2017, accepted 25 October 2017, published online 27 November 2017

Originally submitted to SEGJ 1 October 2016, accepted 22 September 2017

## Introduction

The controlled-source electromagnetic (CSEM) method has been used in the last decade as a tool for exploring marine environments (Constable, 2010; Streich, 2016). For example, this method has been applied to surveys for hydrocarbons (Ellingsrud et al., 2002; Constable and Srnka, 2007; Streich, 2016), gas hydrates (Schwalenberg et al., 2010; Weitemeyer et al., 2011) and a fault system in bending oceanic crust before it sinks into the subduction (Naif et al., 2015). Most data analyses of the CSEM method use forward or inversion schemes to estimate the resistivity structure beneath the earth. These schemes are usually used to fit calculated electromagnetic data to observed electromagnetic data. However, the observed electromagnetic field data are generally noisy and/or biased. In general (on land and seafloor), noise arises from the equipment (Constable, 2013), power grids (Nockles et al., 2009), sporadic noise (Strack et al., 1989), ocean currents (Kasaya and Goto, 2009), airwaves (Løseth et al., 2010; Chen and Alumbaugh, 2011; Wirianto et al., 2011) and so on. Data processing techniques are used to decrease the noise components and to extract interpretable

data from the observed electromagnetic fields and are indispensable in estimating the noise-free response of marine CSEM data. As a result, noise reduction can improve estimations of resistivity structures beneath the surface.

Careful treatment of noise is essential for small-scale CSEM surveys in a hydrothermal area. Exploration around hydrothermal fields is becoming important, as they provide mineral resources of high quality for engineering applications and hydrothermal vent organisms for scientific research. From previous research, hydrothermal vents and mounds are considered to be electrically conductive, as they are a potential resource for metals such as Cu, Zn, Ag and Au (Bartetzko et al., 2006; Spagnoli et al., 2016), although the resistivity structure beneath the seafloor still remains. However, exploration in such areas is difficult for several reasons. One reason is the topography around hydrothermal vents. A hydrothermal vent can create a tall chimney with height of up to 20 m (Delaney et al., 1992). Figure 1 shows the seafloor topography in the Iheya North hydrothermal field in the Okinawa Trough, Japan. The figure also shows the tall chimneys and knolls created by hydrothermal

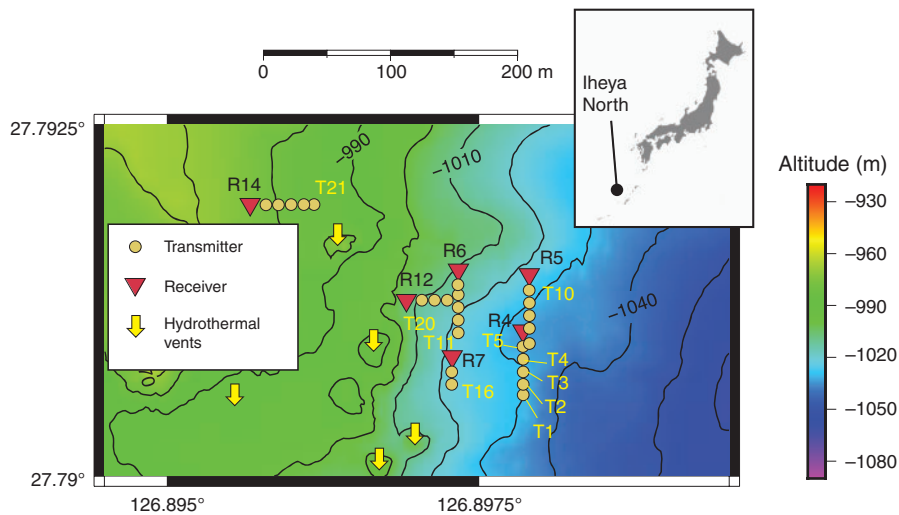


**Fig. 1.** Geometry of the CSEM survey showing the topography of the seafloor with contours and colour. Yellow circles depict ROV transmitters. Red triangles depict OBEM receivers. Identification numbers are shown for several transmitters and receivers. Yellow arrows depict hydrothermal fluid venting sites shown in Kawagucci et al. (2013).

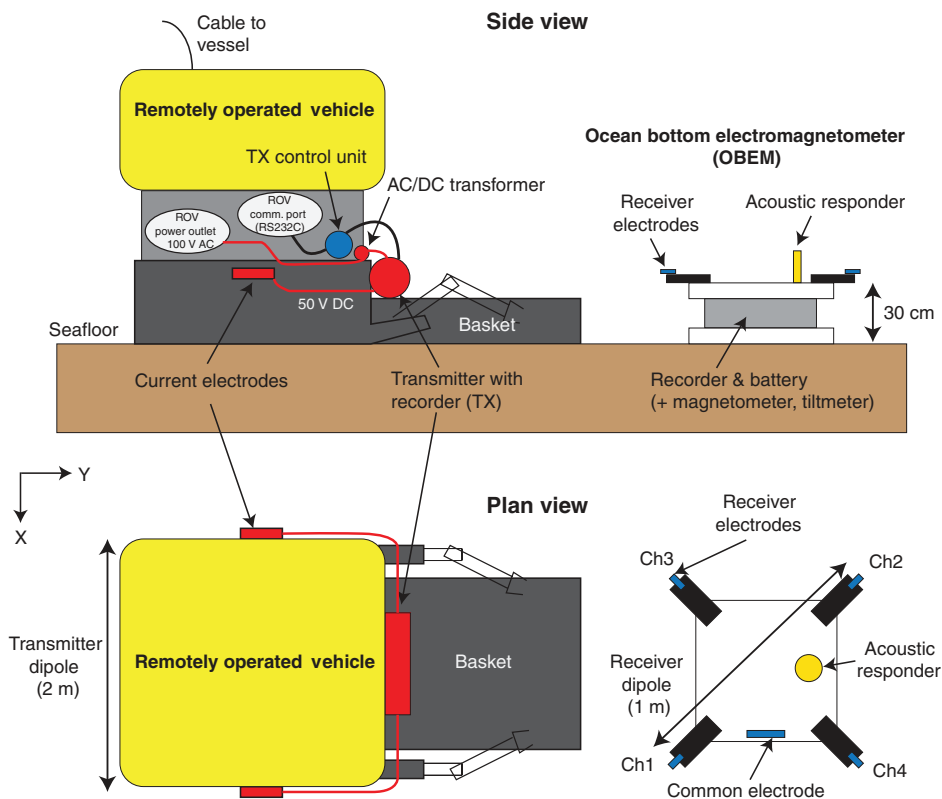


**Fig. 2.** Simplified sketch of the ROV-OBEM system in side and plan views. The ROV transmits electric current after placing the OBEM at the target location. The ROV transmits electric current every 30 s once it has settled on the seafloor.

vents, which form a major part of the topography in this area. This topography makes traditional CSEM surveying, conducted by towing cables, difficult because the cables must be towed far above the chimneys, which reduces the amplitude of the electromagnetic response from the subsurface. Another reason is the limited spatial extent of the hydrothermal fields. Although traditional CSEM methods are used for conducting hydrocarbon surveys covering several kilometres in extent, hydrothermal vents are generally densely distributed over an area of several hundred

metres. Exploration of small spatial extent requires stable and accurate measurement of the positions of transmitters and receivers, which is difficult even with modern survey systems. To solve the above-mentioned problems, we have developed a new CSEM survey system based on a remotely operated vehicle (ROV) and an ocean bottom electromagnetometer (OBEM), as shown in Figure 2. In this system, the ROV brings the OBEM exactly to defined locations in the target area, irrespective of its topography, and the offset between the ROV and the OBEM can

be determined with high accuracy. However, the ROV can handle only small amplitudes of electric current because of its limited output power. Also, the maximum length of the electric dipoles of the ROV and the OBEM should be less than a few metres to ensure portability by the ROV. As such, noise must be decreased by data processing to increase the signal-to-noise ratio.

In marine CSEM data processing, several techniques are used to recover a noise-free response function, which can be a function in either time or frequency domains. Previous CSEM research involves significant efforts to reduce noise to sufficiently low levels (Myer et al., 2011). CSEM data processing typically comprises general digital signal processing steps. However, other processes have been used for different targets, datasets and external field environments. Myer et al. (2012) pre-whitened and post-darkened observed data to suppress spectral leakage caused by the time variations in the Earth's electromagnetic field. Streich et al. (2013) applied robust weighted least square fitting to CSEM data that was part of a magnetotelluric (MT) survey (Egbert and Booker, 1986; Chave and Thomson, 1989), while other research aims to decrease the airwave effect by data processing (Chen and Alumbaugh, 2011).

Recently, independent component analysis (ICA) has been proposed for addressing signal separation problems (Hyvärinen and Oja, 2000; Cichocki and Amari, 2002). This method is used to separate recorded signals that are weighted sums of source signals into those original source signals. In ICA, information about original source signals and their mix is unknown. ICA finds a linear representation of the recorded signals so that the separated source signal estimates are statistically independent, or are as independent as possible. Because we do not know the mixing weights, ICA is called a 'blind source separation' method. An interesting property of ICA is its robustness against outliers in data (Hampel et al., 1986), which is important for robust processing of electromagnetic survey data. ICA has been applied to sound, image and biomedical signal processing and has also been used in geophysical data processing (Aires et al., 2002; Furukawa et al., 2006; Ciaramella et al., 2004; Tsuno and Iwata, 2015). Murakami and Yamaguchi (2007) used ICA for analysing geoelectric data that were subjected to a very high level of noise during a water injection experiment at the Nojima Fault in Japan. Sato et al. (2017) also used ICA for the processing of a self-potential survey dataset to decrease its noise level. Both geoelectric studies show that the noise level could be reduced sufficiently, but as yet there are few applications of ICA to the geoelectromagnetic problem.

In this paper, we first present a new CSEM observation system used in the Iheya North hydrothermal field in the Okinawa Trough. We describe this observation system, which uses a ROV and an OBEM for a small-scale CSEM survey. Next, we explain ICA and the robust data processing algorithm that is applied to the data collected around hydrothermal areas. The electric potential data observed with the OBEM are shown to contain both impulsive noise and high-frequency noise. Our aim is to extract interpretable CSEM signals from the noisy data, focusing on one OBEM dataset. We show the processing results of time series and spectral data without and with ICA. These processed data are normalised using a dataset obtained away from the hydrothermal area to obtain the normalised electric field responses. We then applied a 2D inversion scheme to the electric field data to estimate the resistivity structure beneath the seafloor. Finally, we interpret the resistivity structure of the hydrothermal field and discuss the effectiveness of data processing for the reduction of noise.

## Remotely operated vehicle system

As we mentioned above, we have developed a CSEM survey system using a ROV and an OBEM as shown in Figure 2. The ROV is equipped with an electric transmitter dipole with a length of ~2 m. The amplitude of current is limited to a maximum of 50 A. Trading off desired source power and practicability, we typically transmitted an electric current of rectangular waveform every 30 s, only once the ROV was stationary on the seafloor. We shortened each of the four horizontal receiver arms of the OBEM to 0.3 m to be carried by the ROV. The OBEM then carried two orthogonal dipoles of 1 m length. This arrangement allowed us to set the OBEM exactly in place inside the target area. After installing the OBEM inside the target area (e.g. at R4 in Figure 1), the ROV ran a survey line transmitting an electric current at each station (T1 to T5). The distance between the transmitter (ROV) and the receiver (OBEM) was accurately measured with an acoustic responder. Video and digital still cameras mounted on the ROV captured graphical information while the ROV moved in the area. GPS signals were used for time synchronisation between the transmitter and the OBEM before deployment and for measuring the drift of the OBEM and ROV clocks after their recovery on board.

Although there are four channels of electric potential, relative to a central common electrode attached to the OBEM, one of the channels did not record properly. We therefore used three channels to calculate the horizontal electric field components. As these channels contain high-amplitude periodic noise and high-frequency noise, observed data at far offsets has a very low signal-to-noise ratio (e.g. Figure 3). This periodic noise was thought to arise when observed data were written to the recording media in the OBEM. As each noise impulse has an independent duration in time, removing this noise by applying a moving average filter or a median filter is difficult, and estimation of the noise waveform by stacking the noise pulses was unsuccessful. The observed time series is also contaminated by high-frequency noise, which will be described later. We apply robust processing to the time series to remove the impulsive noise and the high-frequency noise.

## Method

We used ICA and some basic signal processing to reduce the noise in the observed time series. ICA recovers signals only from the measured data. The ICA method is based on a form of signal analysis that uses statistical assumptions to enable blind source separation. In the ICA process, observed data are considered to be composed of linearly superposed mixtures of original signals:

$$\mathbf{x}_{m \times 1} = \mathbf{A}_{m \times n} \mathbf{s}_{n \times 1}, \quad (1)$$

where  $\mathbf{x}$  represents the components of observed data,  $\mathbf{s}$  represents the original signals and  $\mathbf{A}$  is a non-singular mixing matrix. The application of ICA is for the case where  $\mathbf{s}$  and  $\mathbf{A}$  are unknown. Additionally, we define  $\mathbf{y}$  and  $\mathbf{B}$  as follows:

$$\mathbf{y}_{n \times 1} = \mathbf{B}_{n \times m} \mathbf{x}_{m \times 1}, \quad (2)$$

where a matrix  $\mathbf{B}$  can be built by splitting up the measured signals so that the resulting output vector  $\mathbf{y}$  is the optimal approximation of vector  $\mathbf{s}$ . If  $\mathbf{B}$  corresponds to the inverse matrix of  $\mathbf{A}$ , then  $\mathbf{y}$  is the same as  $\mathbf{s}$ . The goal of ICA is to obtain a matrix  $\mathbf{B}$  in such a way that vector  $\mathbf{y}$  is close to the original, independent source signals. An important assumption in ICA is that the components of  $\mathbf{s}$  are statistically independent.

One of the important aspects of ICA is that it is a statistical model. This means that the distribution of a sum of independent random variables becomes a Gaussian distribution

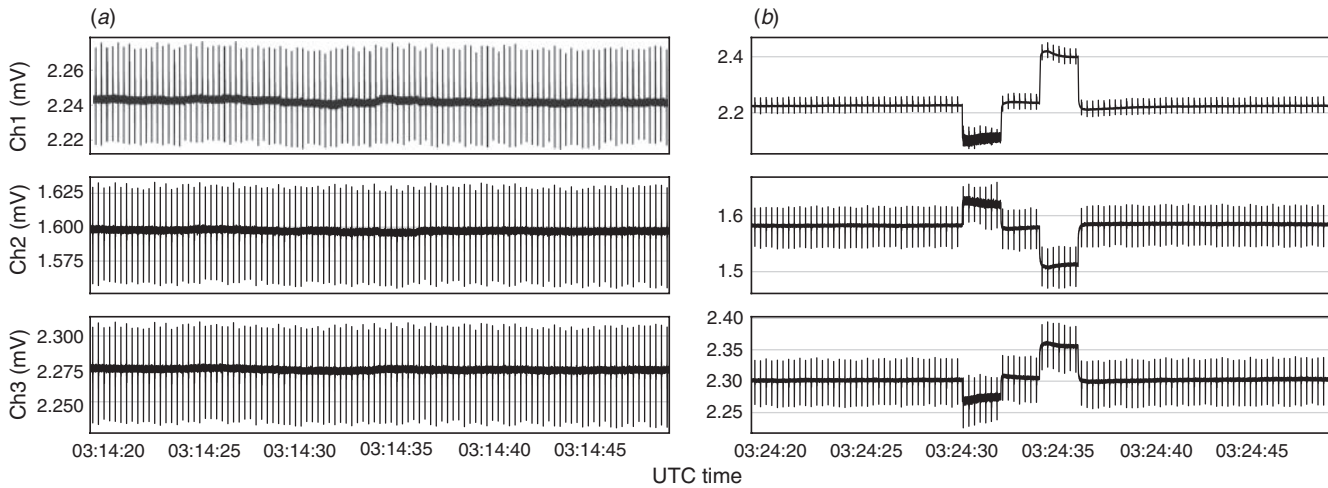


**Fig. 3.** Data examples for receiver R4 and transmitters (a) T1 and (b) T5 with a transmitter–receiver distance of 50 and 10 m, respectively. As one channel in the OBEM did not record the time series of the electric field well, only three channels of data are shown. The source signal is a rectangular waveform with a period of 8 s.

from the central limit theorem. The main idea of ICA is to maximise non-Gaussianity to extract the independent components of signals. In ICA, optimisation is used to maximise non-Gaussianity. A popular optimisation method is FastICA (Hyvärinen and Oja, 2000), which we use here for processing data. FastICA finds a direction  $\mathbf{w}$ , which is one of the rows of the matrix  $\mathbf{B}$ , so that the projection  $\mathbf{w}^T \mathbf{x}$  maximises the independence of the single estimated source  $\mathbf{y}$ . Independence is measured by the approximation of negentropy, which is a measure of non-Gaussianity. We maximise function  $J_G$  to find one independent component:

$$J_G(\mathbf{w}) = \left[ E\{G(\mathbf{w}^T \mathbf{x})\} - E\{G(v)\} \right]^2, \quad (3)$$

where  $\mathbf{w}$  is a weight vector constrained so that  $E\{(\mathbf{w}^T \mathbf{x})^2\} = 1$ ,  $E\{\cdot\}$  indicates the expectation value,  $G$  is a suitable approximating contrast function and  $v$  is a standardised Gaussian random variable. This maximisation requires a whitening of the observed variables. This means that before the application of the ICA algorithm, we transform the observed vector  $\mathbf{x}$  linearly so that we obtain a new vector  $\tilde{\mathbf{x}}$  that is white, i.e. its components are uncorrelated and their variances equal unity with zero mean. To apply the procedure described above, ICA requires the following assumptions for observed data. First, all the sources must be statistically independent of each other. These independent components must be non-Gaussian. Second, the number of observed signals must be at least as large as the number of independent components. Finally, matrix  $\mathbf{A}$  has to be of full column rank.

### Application to field data

We apply robust data processing to the field data acquired from the Iheya North hydrothermal field in the Okinawa Trough during the research cruise ‘NT13-22’ (conducted in November 2013) of R/V *Natsushima*, a JAMSTEC (Japan Agency for Marine–Earth Science and Technology) research vessel. These data were obtained by using the ROV-OBEM survey system loaded on ROV *Hyper-Dolphin*. The recorded electric potential in three channels is shown in Figure 3 with a sampling rate of 1 kHz. As one can see in Figure 3, a periodic impulsive noise contaminates the observed data. The impulses occur approximately every 0.29 s. This delta-like function has a broad spectrum in the frequency domain and causes noise in the whole response spectrum.

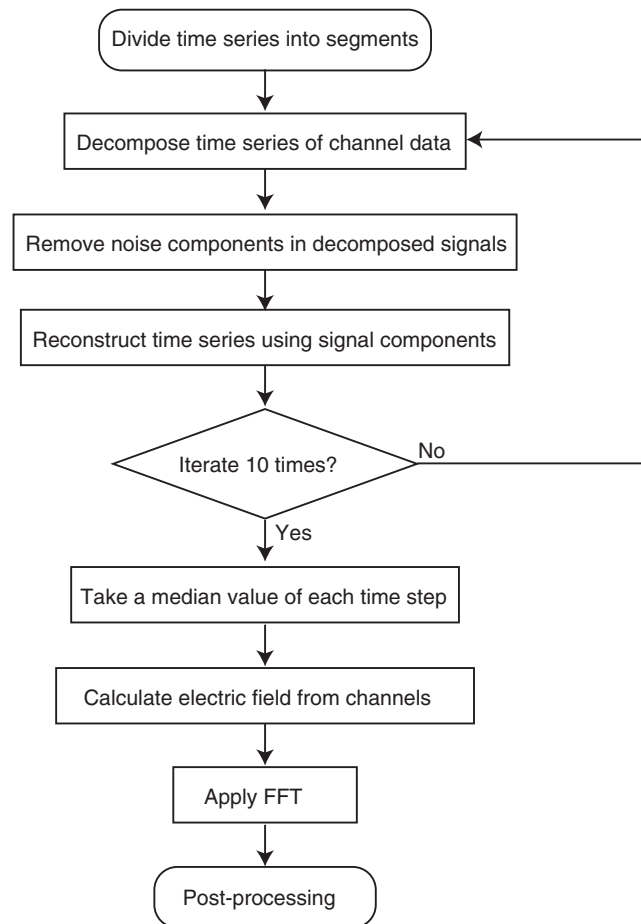


**Fig. 4.** Summary of the statistical data processing scheme. The loop implements the statistical processing algorithm for a given time series of three channels. It reconstructs recovered signals after removing the noise components.

Figure 4 shows a flowchart of our processing scheme. First, we divided the whole time series into segments that each includes a signal generated by the ROV. These time series are decomposed into several independent signals using the ICA algorithm. In this example, we used either two or three independent signals, chosen by a trial-and-error method. Next, we removed the noise

components in the decomposed signals. A decomposed signal was determined to be a noise component if its correlation coefficient with the source signals was not the highest value in the correlation coefficients between the decomposed signals and the source signals. After removing the noise components, the estimated electric potential is recovered using a mixing matrix based on Equation 1.

In the FastICA algorithm, the initial value of  $\mathbf{w}$  is a random value on the unit circle in the coordinate space of whitened observed signals. Convergence of the ICA algorithm depends on the starting value of  $\mathbf{w}$ . As the ICA algorithm can fail its signal decomposition depending on the initial choice of  $\mathbf{w}$ , we apply it 10 times and take the median value for each time step to avoid failure of the ICA algorithm. Figure 5 shows an example of the decomposed signals for the transmitter–receiver pair T5 and R4 (Figure 1). From this figure, it is obvious that the ICA algorithm can decompose original time series into rectangular signal waveforms and impulsive noise components, although there still exists some small impulsive noise in the rectangular signal waveforms. One can see that noise components include both periodic and fluctuating noise in the baseline. However, the amplitude of fluctuating noise is smaller than that of periodic noise. The mixing values of the signal waveform for channels 1, 2 and 3 are 0.0096,  $-0.0036$  and 0.0028, respectively. These channel numbers can be seen in Figure 2. The values for the impulsive noise components are  $-0.0005$ ,  $-0.0006$  and  $-0.0006$  for channels 1–3, respectively. This shows that the mixing values of the impulsive noise have a similar value for each

channel, which in-turn indicates that the impulsive noise comes from an instrumental source and not from the source signal. If this noise were caused by the source current, the mixing value would be different for each channel because the offset is different. This noise reduction process allows us to extract the instrument noise and evaluate its amplitude. Noise-free electric potential channel data are obtained after removing the noise components. When we decomposed the observed signals to three independent signals for the pair T5 and R4, the original rectangular signal waveform was decomposed into two different waveforms contaminated with the noise components. Therefore, we chose to decompose the observed signals to the two signals shown in Figure 5. For the other pairs from T1 to T4 and R4, we decomposed the observed signals to three independent signals. Two components of horizontal electric fields were then calculated from the recovered three-channel data.

Figures 6 and 7 show the electric fields without and with data processing, in the time and frequency domains. These electric fields are the components parallel to the transmitter dipole of the ROV. These observed electric fields and transmitter currents are oriented close to the east–west direction, which is the broadside dipole configuration in the marine CSEM survey. Figure 7a shows that the recovered time series with ICA processing could remove impulsive noise compared with the original time series for the pair T1 and R4. One can see that the amplitude of high-frequency fluctuations in Figure 6a is close to the amplitude of the step in the rectangular wave, although the high-frequency amplitude in Figure 7a is smaller than the amplitude of step in the

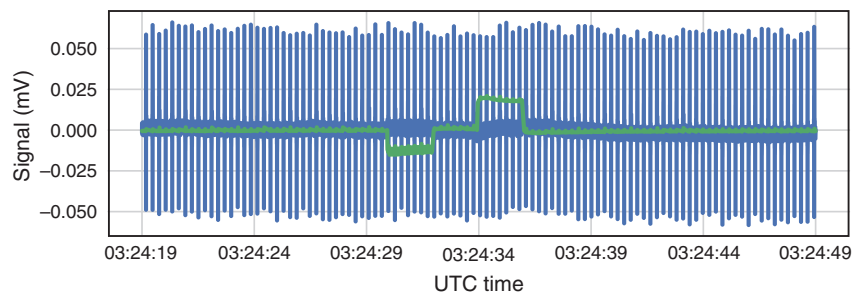


**Fig. 5.** Decomposed signals for transmitter T5 and receiver R4. The blue line depicts the noise component of the time series. The green line depicts the signal component of the time series.

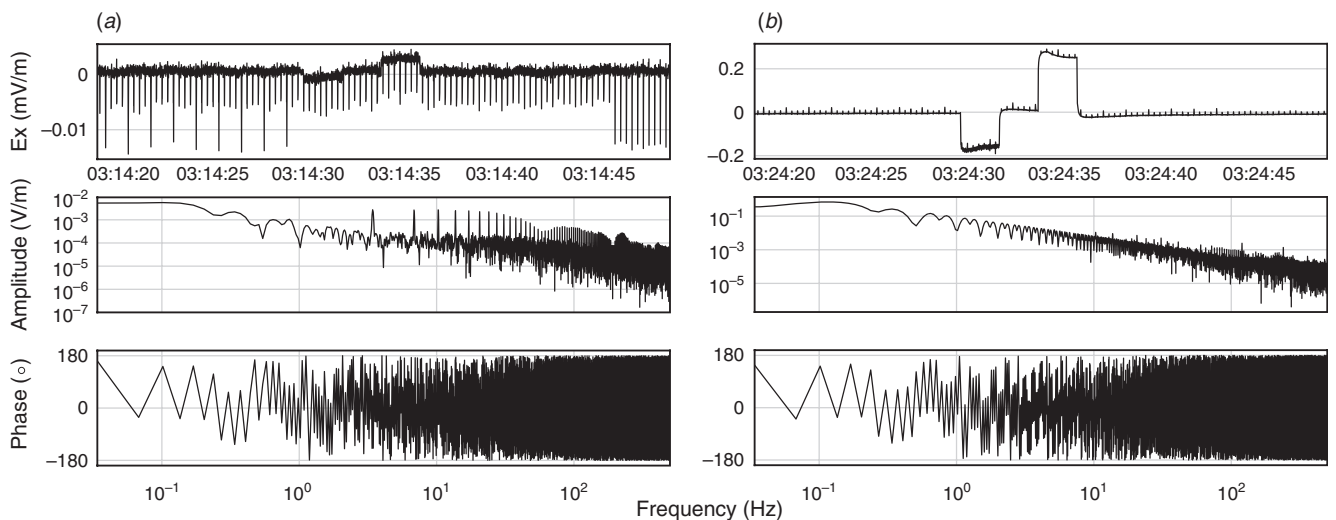


**Fig. 6.** Time series of electric fields, amplitude spectrum of electric field in the frequency domain and phase spectrum (in order from top to bottom). (a) Broadside component of electric field at receiver R4 from transmitter T1 and (b) broadside component of electric field at receiver R4 from transmitter T5.

rectangular wave. As the original source signal does not have these fluctuating signals, they are considered to be high-frequency noise caused during observation and are reduced successfully. Figure 7b shows that their time series do not change before and after data processing. This is because the mixed value of noise in this pair is small compared with the rectangular signal components (Figure 5). This suggests that ICA processing could decompose the impulsive noise and high-frequency noise if its amplitude is large enough compared with the amplitude of the rectangular signal.

The spectra of the T1-R4 pair without and with ICA are different across the whole frequency range (Figures 6a and 7a). It is obvious that the impulsive noise in the time series affects a broad range of frequencies. It can be observed that the spectrum is close to flat from 1 to 100 Hz in Figure 6a. This frequency band corresponds to the periodic impulsive noise in the time series. On the other hand, the spectrum with ICA is not flat in the same frequency band since it does not have a high-amplitude impulse.

The spectrum of the T5-R4 pair without and with ICA does not change much (Figures 6b and 7b) because each time series is similar to the other.

We applied this ICA processing scheme to all datasets (T1, T2, T3, T4 and T5) for receiver R4. Figure 8 shows the amplitude and phase of the spectrum of the broadside electric field as a function of frequency and distance between the ROV and the OBEM. Note that the spectrum of the electric field is Green's function, which is normalised by the transmitted source spectrum. From this figure, one can see that the spectrum is similar at low frequencies without (Figure 8a, b) and with (Figure 8c, d) ICA processing. However, the spectra at middle-to-high frequencies are largely different from Figure 8a, c. This is the same for the phase spectrum as well. These trends are explained by the same reason given above. As the impulsive noise in the time series affects largely the middle-to-high frequency range, the spectra in these regions are contaminated. One can also see that the processed spectrum becomes smoother in space compared with the result

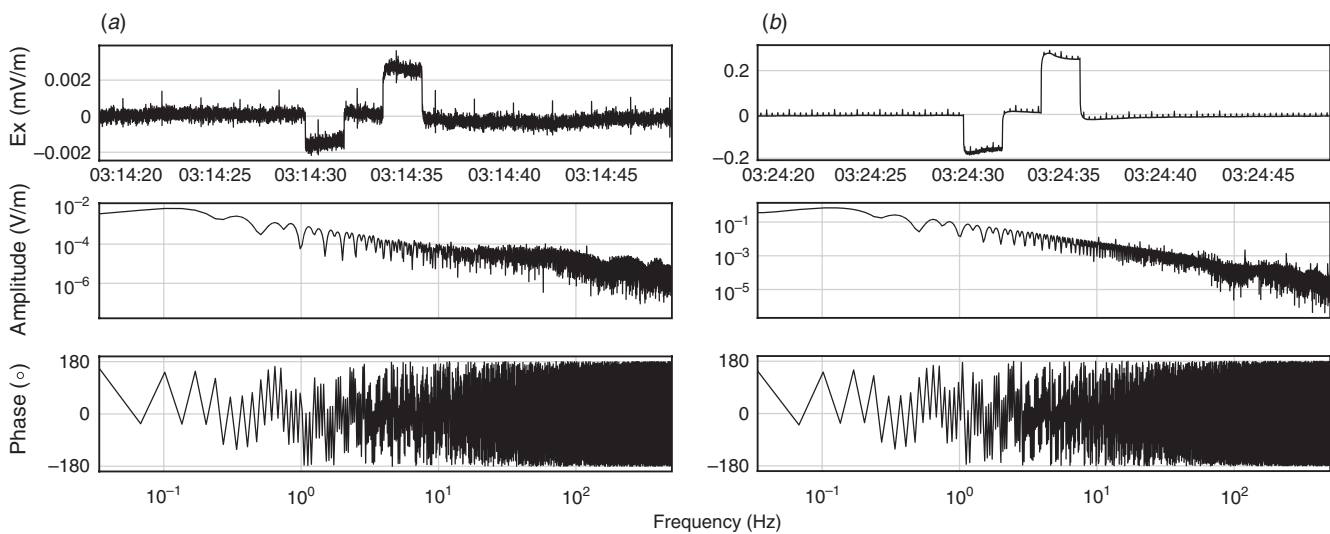


**Fig. 7.** Time series of electric fields, amplitude spectrum of electric field in the frequency domain and phase spectrum (in order from top to bottom) after the ICA algorithm has been applied. (a) Broadside component of electric field at receiver R4 from transmitter T1 and (b) broadside component of electric field at receiver R4 from transmitter T5.

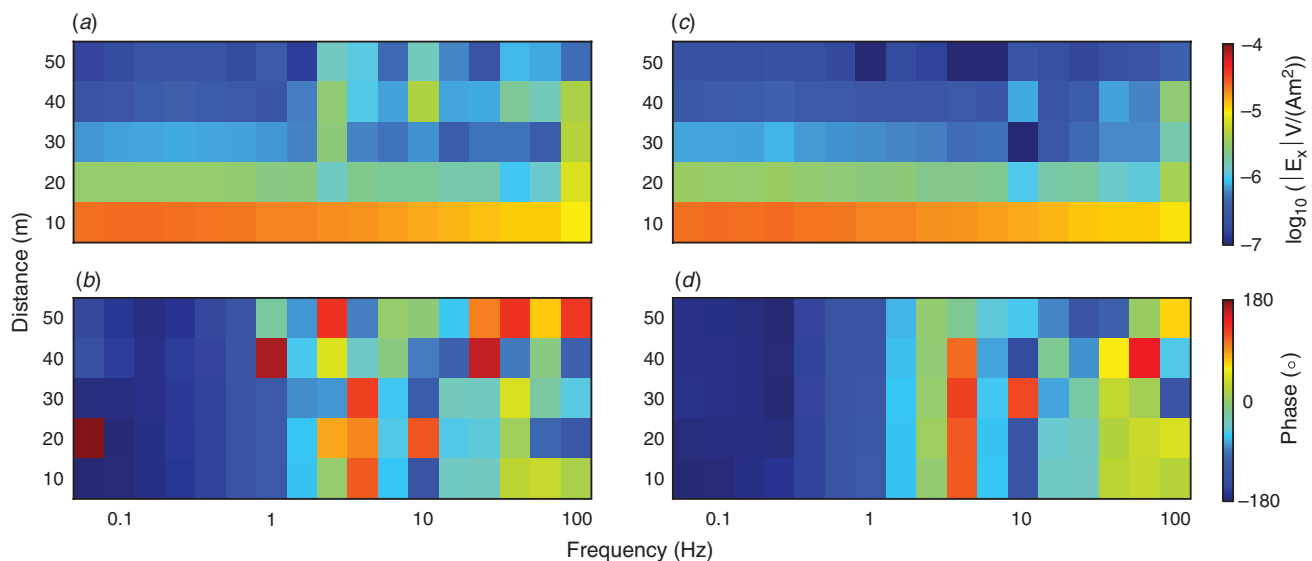


**Fig. 8.** Responses at receiver R4 for all of the transmitters: (a, b) without ICA processing and (c, d) with ICA processing applied. Amplitude spectra are shown in (a, c) and phase spectra in (b, d).

without ICA processing (Figure 8). This smooth spectrum is considered to be reasonable because electromagnetic fields are governed by the diffusion equation, which makes the distribution of the spectrum smooth in space under the noise-free condition.

We normalised these spectrum amplitudes by the responses obtained outside the hydrothermal area using the same survey system (the site location is 1.5 km east of the target area in Figure 1). The normalised spectrum is calculated by dividing the amplitude of the spectrum in Figure 8 with the amplitude of the spectrum from the remote area. This provides us with an apparent resistivity map because the normalised spectrum decreases the diffusive attenuation of the observed electromagnetic fields.

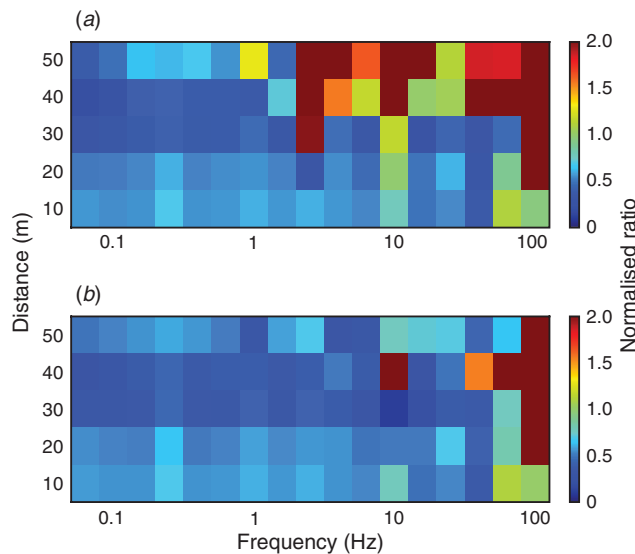


**Fig. 9.** Normalised responses at receiver R4 (a) without ICA processing and (b) with ICA processing applied.

Figure 9a and b show the normalised spectrum without and with ICA processing, respectively. From the results, we find that the non-processed response has a larger normalised ratio than the processed response at middle-to-high frequencies. This means that the non-processed response indicates larger electric fields at these frequency bands. However, these apparently larger electric fields are artefacts, generated by the impulsive and environmental noise. After data processing, we obtained a lower normalised ratio, indicating that the resistivity in this area is low, which is reasonable for a hydrothermal area. As this normalised ratio represents apparent resistivity, a higher frequency reflects the resistivity at shallow depth and a lower frequency reflects the resistivity structure at greater depth. From Figure 9b, one can see that the resistivity is low in the deep area.

To confirm this interpretation, we applied 2D inversion to the observed data using MARE2DEM (Key, 2016). Broadside electric field responses were computed at four frequencies: 0.13, 0.50, 2.00 and 7.97 Hz, which are similar to the period of the transmitted rectangle waveform. Since these frequencies are low considering the skin depth for the target area, the resolution of the structure is not high. We used the topography around the observation area, which has 2 m resolution in the horizontal direction, to define the model interface. The initial model consists of seawater with a resistivity of  $0.3125 \Omega\text{m}$  and a half-space with a resistivity of  $10 \Omega\text{m}$ . Figure 10a and b show the inversion results without and with ICA processing, respectively. Both inversion results converged with a target root mean square (rms) misfit 1.0 after 18 and 11 iterations, respectively. The inversion result without ICA processing depicts an extremely high-resistivity body beneath the seafloor around T4 and T5 (feature A). This resistive body continues to the location of the OBEM. The inversion result with ICA processing also shows a high-resistivity body in a similar place, but its size is smaller than the one without ICA processing and is limited to shallow depths. Both inversion results image low resistivity bodies under the

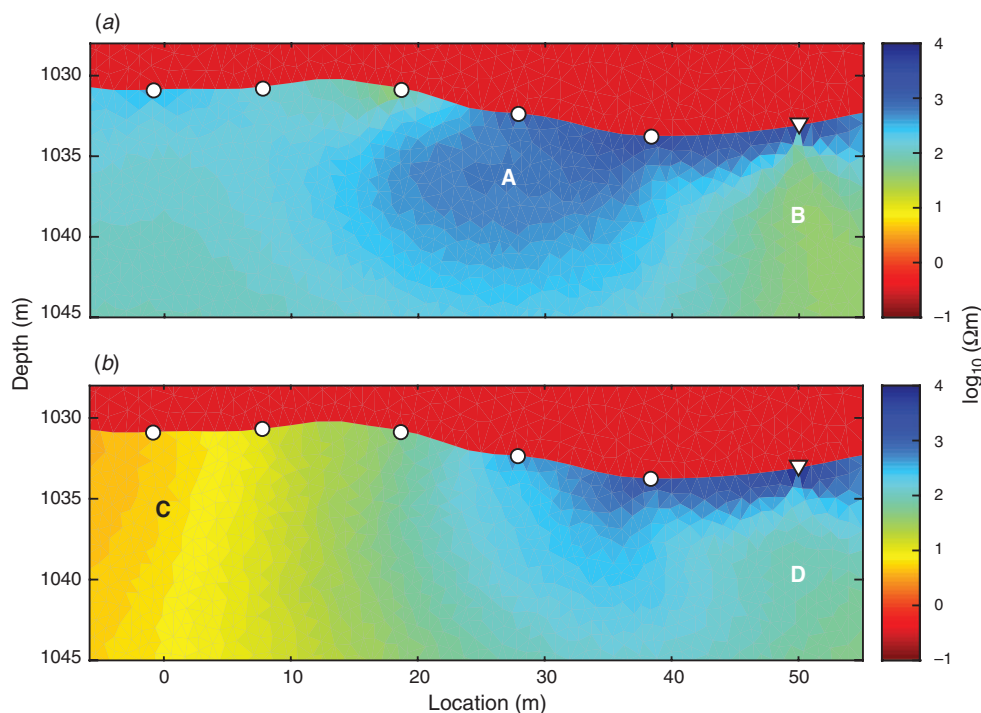


**Fig. 10.** Resistivity model of the inversion results (a) without ICA processing and (b) with ICA processing applied. Five white dots depict the location of transmitters (T1 to T5) and a white triangle depicts the location of the receiver (R4). Labelled features include resistive shallow accumulations (A) and conductive bodies (B, C and D).

resistive shallow sediment near the OBEM (features B and D). The size and the resistivity of these features are similar to each other. It seems that this low resistive body continues up to the seafloor. There is another low-resistivity body beneath T1 and T2 in Figure 10b. Its resistivity is ~10 times lower than the same location in Figure 10a. Overall, it appears that the resistivities without ICA processing are larger than those with ICA processing. The reason for this can be explained from Figure 8. This figure shows that the amplitude of the spectrum without ICA processing is larger than the one with ICA processing. The extremely high-resistive zone (A in Figure 10a) is a result of the larger amplitude of the spectrum obtained without ICA processing and is probably a false structure, perhaps due to spike noise in the observed time series.

Since the *in situ* resistivity is still unknown in this target region, as far as the authors know, further discussion of the distribution of conductive hydrothermal fluids or deposits should be based on core samples. Here, we made a preliminary interpretation based on photographs taken by the ROV. From the photos, hydrothermal fluid and gas seepage from the seafloor appears between R4 and T5 (~10 m wide). Characteristic bacteria and mussels, typical organisms found at hydrothermal seepages, are also seen around the area. The inversion results from Figure 10 show the low resistivity around the location of the seepage (features B and D). The photos also show that there are characteristic mussels in colonies on the left side, far from T1. This might support the conclusion that the inversion result with ICA processing (feature C; Figure 10b) is more reasonable than the one without ICA processing (Figure 10a), which has a higher resistivity in the same area.

## Conclusion

We have presented the ICA method for robust processing of data obtained around the Iheya North hydrothermal field, Okinawa Trough, Japan. The data was collected in 2013 using a newly developed CSEM survey method based on a ROV-OBEM system, which is useful for both small-scale surveys and surveys in areas of steep topography. In the electric potential data obtained, there is periodic and environmental noise, which makes the interpretation of observed data difficult. After robust processing of the data, we found that impulsive and environmental noise components could be reduced effectively. As a result, the spectrum of electric fields with ICA looks reasonable, especially at middle-to-high frequencies, compared with the spectrum without ICA. The spectrum of electric fields was normalised using a spectrum from data acquired away from the hydrothermal areas. This normalised ratio shows that the apparent resistivity is low at shallow depths around the OBEM location. The inversion results also show that low resistivity bodies exist beneath the OBEM and stations T1 and T2. The location of the resistivity anomaly is also consistent with images taken by the ROV, which show seepage with typical hydrothermal vent organisms in the same area. The applications of the robust processing method described here are not limited to CSEM data. Noise in time series data can be reduced in a similar manner for different types of survey such as MT surveys, direct current surveys and transient electromagnetic surveys.

## Conflicts of interest

The authors declare no conflicts of interest.

## Acknowledgements

The authors thank the two anonymous reviewers for their fruitful suggestions and comments. They are grateful for the many efforts and kindness of Hiroyuki

Yamamoto, JAMSTEC, Chief Scientist on the NT13–22 cruise. The authors also thank the Captain, crew and technicians of R/V *Natsushima*, the operating team of ROV *Hyper-Dolphin* and supporting members for their cooperation. This project is supported by MEXT (Ministry of Education, Culture, Sports, Science and Technology of Japan), in a development program of fundamental tools for exploration of deep seabed resources, and partly by JSPS KAKENHI Grant Numbers 26289347, 26249060, 26282101, 15H03715 and 15H05815.

## References

- Aires, F., Rossow, W. B., and Chédin, A., 2002, Rotation of EOFs by the independent component analysis: toward solving the mixing problem in the decomposition of geophysical time series: *Journal of the Atmospheric Sciences*, **59**, 111–123. doi:10.1175/1520-0469(2002)059<0111:ROEBT>2.0.CO;2
- Bartetzko, A., Klitzsch, N., Iturrino, G., Kaufhold, S., and Arnold, J., 2006, Electrical properties of hydrothermally altered dacite from the PACMANUS hydrothermal field (ODP Leg 193): *Journal of Volcanology and Geothermal Research*, **152**, 109–120. doi:10.1016/j.jvolgeores.2005.10.002
- Chave, A. D., and Thomson, D. J., 1989, Some comments on magnetotelluric response function estimation: *Journal of Geophysical Research*, **94**, 14215–14225. doi:10.1029/JB094iB10p14215
- Chen, J., and Alumbaugh, D. L., 2011, Three methods for mitigating airwaves in shallow water marine controlled-source electromagnetic data: *Geophysics*, **76**, F89–F99. doi:10.1190/1.3536641
- Ciaramella, A., Lauro, E. D., Martino, S. D., Lieto, B. D., Falanga, M., and Tagliaferrri, R., 2004, Characterization of Strombolian events by using independent component analysis: *Nonlinear Processes in Geophysics*, **11**, 453–461. doi:10.5194/npg-11-453-2004
- Cichocki, A., and Amari, S., 2002, *Adaptive blind signal and image processing*: John Wiley & Sons, Inc.
- Constable, S., 2010, Ten years of marine CSEM for hydrocarbon exploration: *Geophysics*, **75**, 75A67–75A81. doi:10.1190/1.3483451
- Constable, S., 2013, Review paper: Instrumentation for marine magnetotelluric and controlled source electromagnetic sounding: *Geophysical Prospecting*, **61**, 505–532. doi:10.1111/j.1365-2478.2012.01117.x
- Constable, S., and Srnka, L. J., 2007, An introduction to marine controlled-source electromagnetic methods for hydrocarbon exploration: *Geophysics*, **72**, WA3–WA12. doi:10.1190/1.2432483
- Delaney, J. R., Robigou, V., McDuff, R. E., and Tivey, M. K., 1992, Geology of a vigorous hydrothermal system on the Endeavour Segment, Juan de Fuca Ridge: *Journal of Geophysical Research*, **97**, 19663–19682. doi:10.1029/92JB00174
- Egbert, G. D., and Booker, J. R., 1986, Robust estimation of geomagnetic transfer functions: *Geophysical Journal of the Royal Astronomical Society*, **87**, 173–194. doi:10.1111/j.1365-246X.1986.tb04552.x
- Ellingsrud, S., Eidesmo, T., Sinha, M. C., MacGregor, L. M., and Constable, S., 2002, Remote sensing of hydrocarbon layers by Seabed Logging (SBL): results from a cruise offshore Angola: *The Leading Edge*, **21**, 972–982. doi:10.1190/1.1518433
- Furukawa, A., Kimono, J., and Otsuka, H., 2006, Development of response extraction technique using ICA and its application to structural damage identification: *Journal of Applied Mechanics*, **9**, 43–54. [in Japanese] doi:10.2208/journalam.9.43
- Hampel, F. R., Ronchetti, E. M., Rousseeuw, P. J., and Stahel, W. A., 1986, *Robust statistics: the approach based on influence functions*: John Wiley & Sons, Inc.
- Hyvärinen, A., and Oja, E., 2000, Independent component analysis: algorithms and applications: *Neural Networks*, **13**, 411–430. doi:10.1016/S0893-6080(00)0026-5
- Kasaya, T., and Goto, T., 2009, A small ocean bottom electromagnetometer and ocean bottom electrometer system with an arm-folding mechanism: *Exploration Geophysics*, **40**, 41–48. doi:10.1071/EG08118
- Kawagucci, S., Miyazaki, J., Nakajima, R., Nozaki, T., Takaya, Y., Kato, Y., Shibuya, T., Konno, U., Nakaguchi, Y., Hatada, K., Hirayama, H., Fujikura, K., Furushima, Y., Yamamoto, H., Watsuji, T., Ishibashi, J., and Takai, K., 2013, Post-drilling changes in fluid discharge pattern, mineral deposition, and fluid chemistry in the Iheya North hydrothermal field, Okinawa Trough: *Geochemistry, Geophysics, Geosystems*, **14**, 4774–4790. doi:10.1002/2013GC004895

- Key, K., 2016, MARE2DEM: a 2-D inversion code for controlled-source electromagnetic and magnetotelluric data: *Geophysical Journal International*, **207**, 571–588. doi:10.1093/gji/ggw290
- Løseth, L. O., Amundsen, L., and Jenssen, A. J. K., 2010, A solution to the airwave-removal problem in shallow-water marine EM: *Geophysics*, **75**, A37–A42. doi:10.1190/1.3475359
- Murakami, H., and Yamaguchi, S., 2007, Extraction of small geoelectric signals from noisy geoelectric data using independent component analysis: *Geoinformatics*, **18**, 29–37. [in Japanese] doi:10.6010/geoinformatics.18.29
- Myer, D., Constable, S., and Key, K., 2011, Broadband waveforms and robust processing for marine CSEM surveys: *Geophysical Journal International*, **184**, 689–698. doi:10.1111/j.1365-246X.2010.04887.x
- Myer, D., Constable, S., Key, K., Glinsky, M. E., and Liu, G., 2012, Marine CSEM of the Scarborough gas field, part 1: experimental design and data uncertainty: *Geophysics*, **77**, E281–E299. doi:10.1190/geo2011-0380.1
- Naif, S., Key, K., Constable, S., and Evans, R. L., 2015, Water-rich bending faults at the Middle America Trench: *Geochemistry, Geophysics, Geosystems*, **16**, 2582–2597. doi:10.1002/2015GC005927
- Nockles, V. A., Wright, D., and Ziolkowski, A., 2009, Power line noise removal techniques for transient electromagnetic data: 71st Annual International Conference and Exhibition, EAGE, Extended Abstracts, P253.
- Sato, S., Goto, T., Kasaya, T., Kawada, Y., Iwamoto, H., and Kitada, K., 2017, Noise reduction method of marine spontaneous electric field data using independent component analysis: *Butsuri Tansa*, **70**, 42–55. [in Japanese] doi:10.3124/segj.70.42
- Schwalenberg, K., Haeckel, M., Poort, J., and Jegen, M., 2010, Evaluation of gas hydrate deposits in an active seep area using marine controlled source electromagnetics: results from Opouawe Bank, Hikurangi Margin, New Zealand: *Marine Geology*, **272**, 79–88. doi:10.1016/j.margeo.2009.07.006
- Spagnoli, G., Hannington, M., Bairlein, K., Hördt, A., Jegen, M., Petersen, S., and Laurila, T., 2016, Electrical properties of seafloor massive sulfides: *Geo-Marine Letters*, **36**, 235–245. doi:10.1007/s00367-016-0439-5
- Strack, K. M., Hanstein, T. H., and Eilenz, H. N., 1989, LOTEM data processing for areas with high cultural noise levels: *Physics of the Earth and Planetary Interiors*, **53**, 261–269. doi:10.1016/0031-9201(89)90010-1
- Streich, R., 2016, Controlled-source electromagnetic approaches for hydrocarbon exploration and monitoring on land: *Surveys in Geophysics*, **37**, 47–80. doi:10.1007/s10712-015-9336-0
- Streich, R., Becken, M., and Ritter, O., 2013, Robust processing of noisy land-based controlled-source electromagnetic data: *Geophysics*, **78**, E237–E247. doi:10.1190/geo2013-0026.1
- Tsuno, S., and Iwata, Y., 2015, Investigation of waveform separation by Independent Component Analysis for composite signals as a target for mixed signals of earthquake ground motions and railway-induced ground vibrations: *Butsuri-Tansa (Geophysical Exploration)*, **68**, 39–47. [in Japanese with English abstract] doi:10.3124/segj.68.39
- Weitemeyer, K. A., Constable, S., and Tréhu, A. M., 2011, A marine electromagnetic survey to detect gas hydrate at Hydrate Ridge, Oregon: *Geophysical Journal International*, **187**, 45–62. doi:10.1111/j.1365-246X.2011.05105.x
- Wirianto, M., Mulder, W. A., and Slob, E. C., 2011, Exploiting the airwave for time-lapse reservoir monitoring with CSEM on land: *Geophysics*, **76**, A15–A19. doi:10.1190/1.3560157